

November 2007

Peptide ormosils as cellular substrates

Sabrina Jedlicka

Purdue University, sjedlick@purdue.edu

Kenneth M. Little

Purdue University, klittle@purdue.edu

David E. Nivens

Purdue University, dnivens@purdue.edu

Dmitry Zemlyanov

Birck Nanotechnology Center, Purdue University, dimazemlyanov@purdue.edu

Jenna L. Rickus

Purdue University, rickus@purdue.edu

Follow this and additional works at: <http://docs.lib.purdue.edu/nanopub>

Jedlicka, Sabrina; Little, Kenneth M.; Nivens, David E.; Zemlyanov, Dmitry; and Rickus, Jenna L., "Peptide ormosils as cellular substrates" (2007). *Birck and NCN Publications*. Paper 281.

<http://docs.lib.purdue.edu/nanopub/281>

This document has been made available through Purdue e-Pubs, a service of the Purdue University Libraries. Please contact epubs@purdue.edu for additional information.

Peptide ormosils as cellular substrates†

Sabrina S. Jedlicka,^{ab} Kenneth M. Little,^c David E. Nivens,^c Dmitry Zemlyanov^{df} and Jenna L. Rickus^{*abe}

Received 16th April 2007, Accepted 24th October 2007

First published as an Advance Article on the web 14th November 2007

DOI: 10.1039/b705393b

Peptide-functionalized thin films exhibit significant potential for integration into implantable devices and cell-based technologies. A new type of neuroactive peptide-modified silica was developed using sol–gel reaction chemistry to produce thin films from four different peptide silane precursors. Peptide silanes containing binding sequences from laminin (YIGSR and KDI), fibronectin (RGD), and EGF repeats from laminin and tenascin (NID) were produced using standard solid-state Fmoc peptide synthesis conditions and the covalent attachment of 3'-(aminopropyl)trimethoxysilane (APTMS), using carbonyldiimidazole (CDI) as a linking molecule. Precursor formation was confirmed with MALDI-MS. Thin films were produced by dip-coating using the peptide precursors combined with hydrolyzed tetramethoxysilane. Atomic force microscopy indicated that the surface topography was not affected by low concentrations of peptide precursor (0.0025 mol%), but higher concentrations of peptide precursor (0.01 mol%) resulted in features that were 50–75 nm in height. The height features observed were consistent in size with previously determined topographical morphology supportive of neuronal cell lines. The surfaces were biologically active and modulated the phenotype of the embryonic carcinoma stem cell line, P19. Combinations of the peptide silanes resulted in altered cell types after retinoic acid treatment. More neurons were observed on RGD/YIGSR and RGD/YIGSR/NID surfaces compared to tetramethoxysilane (TMOS) controls. More supporting cells were observed compared to collagen coated tissue culture plates. In addition, neurites were significantly longer on the peptide ormosils compared to controls. This work demonstrates a novel method for producing biologically active peptide ormosils using peptide-modified precursors.

Introduction

In vivo, neural stem cells are confined to localized regions, or niches, where rich extracellular biological cues contribute to the maintenance, proliferation, and commitment of these cells.^{1,2} During development, these cues help to guide cells down specialization paths to mature phenotypes. While knowledge of stem cell niches is far from complete, current research suggests that extracellular proteins contribute in synergistic and concentration dependent ways. Biologically rich but well-defined, *in vitro* environments will be important tools for the development of neural stem cell technologies and therapeutics.

Surfaces presenting peptide sequences from extracellular matrix and cell–cell adhesion proteins can modulate cell fate and function. Many biomaterial studies implementing peptide chemistry have been based on peptide amphiphiles and

self-assembled monolayers.^{3–13} Such materials are powerful model systems and excellent biomimetics; however a lack of stability over time and at air and organic solvent interfaces currently limits this approach for some applications. This paper describes a sol–gel based peptide material as a potential alternative to self-assembled systems.

The sol–gel method of producing organically modified silica (ormosil) provides a particularly attractive platform for creating biological functionality, as the materials can be doped with a wide variety of organic polymers, biological molecules,^{14,15} biomolecular structures,^{16–18} and living cells.^{19,20} In addition, covalent modification by manipulation of the starting precursor chemistry is possible.²¹ The highly porous network enables the diffusion of small molecules for sensing and controlled release. Because the gels do not swell, they are an excellent alternative to hydrogels in applications where the leaching of pore contents cannot be tolerated. The materials are optically transparent allowing for the integration of materials with traditional and emerging cytomic tools such as laser scanning adherent cell cytometers.²²

Both native and polymer doped sol–gel produced silica thin films can support cell attachment and growth when the physiochemical surface properties are permissive.^{23,24} Many applications, however, will require a more specific presentation of biological cues. Defining direction of cell fate and function using a materials approach, therefore, requires a method for presenting multiple peptides and an ability to control each peptide surface concentration independently.

^aDepartment of Agricultural and Biological Engineering, Purdue University, West Lafayette, IN, USA

^bPhysiological Sensing Facility at the Bindley Bioscience Center, Purdue University, West Lafayette, IN, USA

^cDepartment of Food Science, Purdue University, West Lafayette, IN, USA

^dBirck Nanotechnology Center, Purdue University, West Lafayette, IN, USA

^eWeldon School of Biomedical Engineering, Purdue University, West Lafayette, IN, USA

^fMaterials and Surface Science Institute, University of Limerick, Limerick, Ireland

† Electronic supplementary information (ESI) available: Phase traces from AFM imaging. See DOI: 10.1039/b705393b

To enable a simple and generic method for expression of multiple peptides at the surface of a material, we have developed a “one-pot synthesis” method. This work takes advantage of the ability to form solid-state glasses from liquid silanes using sol–gel reaction chemistry. The technique allows for the production of porous organically modified materials whose surface and pores are decorated by the organic moieties of the starting precursors. Peptides are covalently linked to a silane precursor during synthesis, allowing for the covalent incorporation of these peptides into a silica sol–gel matrix.

We developed the peptide silanes by the covalent attachment of 3'-(aminopropyl)trimethoxysilane (APTMS), using carbonyldiimidazole (CDI) as a linking molecule. This linkage at the N-terminal end of the growing peptide was the last step in a standard solid-state Fmoc peptide synthesis before peptide cleavage from the resin. The linkage and peptide molecular weight was confirmed with MALDI-MS and supported by XPS. Peptide silanes were designed based on known binding sequences of the extracellular matrix proteins fibronectin, laminin and tenascin. The precursors were used in combination with tetramethoxysilane (TMOS) to produce thin films that were then characterized using atomic force microscopy (AFM) and X-ray photoelectron spectroscopy (XPS). The

biological functionality of the films and their ability to modulate the cellular phenotype were confirmed using the embryonic carcinoma stem cell line P19.

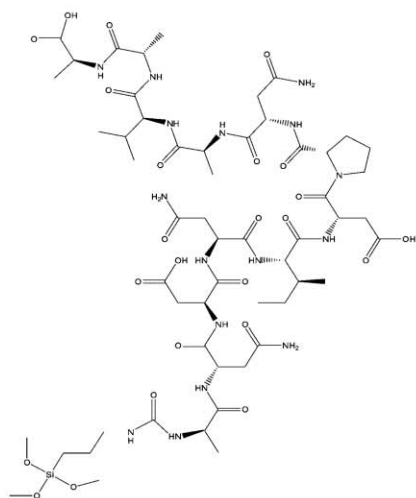
Results and discussion

Peptide silane synthesis

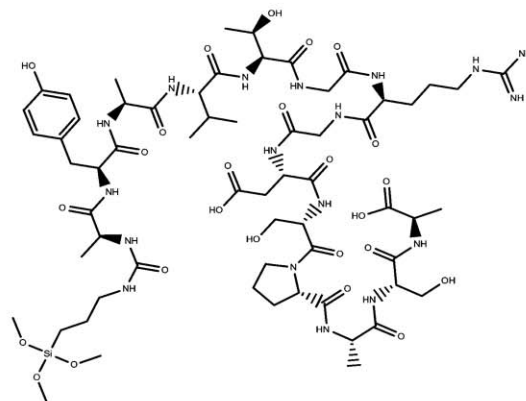
Peptide silanes were synthesized and then characterized using MALDI-MS. The peptide silanes were compared to free peptides to obtain fractionation characteristics of the precursors of interest. Fig. 1 shows the structures of the four peptide silanes created. Table 1 provides the sequence of the four unmodified peptides along with their natural source proteins.

The four peptides were chosen for their known biological functions in neuronal development. The YIGSR (denoted YIG in data) and RGD peptides are cell binding regions found in the extracellular matrix proteins fibronectin and laminin, and are commonly employed in biomaterial surfaces to improve cell adhesion and survival on artificial materials.^{25–27} The KDI sequence directs cellular migration, facilitates axon guidance, and enhances the formation of basic neuronal architecture.²⁸ The NID peptide sequence is a common EGF repeat found in

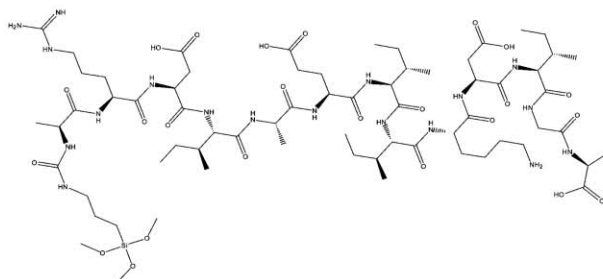
NID Silane



RGD Silane



KDI Silane



YIG Silane

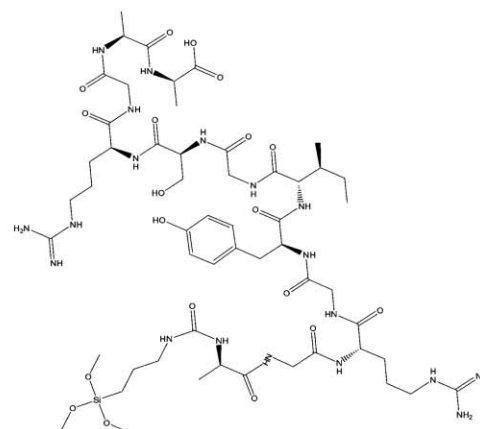


Fig. 1 Structures of peptide silane precursors.

Table 1 Peptides chosen for study. Peptides were chosen to represent the developing embryonic neural environment. Bold residues indicate cell binding sequences

Peptide sequence	Name	Origin	Function	Ref.
AND NID PNAAVAA	NID	EGF repeat laminin, tenascin	Basement membrane organization	Garwood <i>et al.</i> ²⁹
AYAV TGRGD SPASA	RGD	Fibronectin type III repeat	Adhesion, synapse formation	Ruoslahti ²⁶
ARDIAE IKD IGA	KDI	Laminin	Migration, guidance, neuronal architecture	Liesi <i>et al.</i> ²⁸
ADPG YIG SRGAA	YIG	Laminin	Adhesion, synapse formation	Ranieri <i>et al.</i> ²⁷

the extracellular matrix proteins laminin and tenascin,²⁹ which contribute to the neural stem cell niche within the sub-ventricular zone and modulate the effects of growth factors.³⁰

Peptides with a longer sequence length than simply the primary bioactive peptide were used, as they are more likely to mimic the natural conformations found in extracellular matrix (ECM) protein secondary structure. Flanking amino acids were determined from the native protein sequence, and an alanine was added to the C-terminus during synthesis through the use of a pre-conjugated Wang-Ala resin. In addition a minor modification to the N-terminus by the addition of an alanine improved the overall linkage capability of the CDI/APTMS terminating group.

MALDI-MS was used to characterize the average *m/z* ratios of the resulting peptide silanes. The peptides and peptide silanes were partially purified through multiple ether extractions and subjected to standard MALDI conditions. The free peptides and peptide silanes of each sequence of interest were analyzed for comparison and are presented in Table 2. The nominal molecular mass is given for reference. Many of the peptide silanes appear to have undergone partial hydrolysis of the APTMS methyl groups. This hydrolysis is expected, given the trifluoroacetic acid conditions used for peptide cleavage from the resin. The first few products of the MALDI-MS spectra are shown for each sequence with the dominant cleavage product indicated. The molecular ions generated for each sequence product are within experimental limits of the expected nominal molecular mass, demonstrating a successful

conjugation of the APTMS with the CDI linker. There are, however, some minor peaks associated with each of the samples that potentially signal the incomplete removal of amino acid protective groups. While this was not a major consideration for the scope of this project, these artifacts can be removed through a longer TFA treatment and the use of specific scavengers for the protective groups used with the peptide synthesis in future work. Overall, the MALDI-MS data confirm that the peptide is conjugating effectively to the APTMS molecule, and that the peptides themselves are of an expected molecular mass given the chosen sequence. As this technique is developed further for potential therapeutic applications, a more sensitive technique, such as LC-ESI-MS/MS, will need to be applied to confirm peptide sequence and purity.

MALDI-MS was chosen as an analysis technique for these molecules over the traditional silane characterization techniques of nuclear magnetic resonance spectroscopy and Fourier-transform infrared spectroscopy (FT-IR)²¹ due to the peptide-based nature of the molecular structure and the tendency for hydrolysis under acid cleavage. FT-IR was initially used for basic analysis of the peptides (data not shown), however, this method could not be used for confirmation of conjugation due to the carbon fingerprint region overlap with the identifying Si-O peak (1000–1100 cm⁻¹). Additionally, X-ray photoelectron spectroscopy (XPS) was used for surface analysis of the peptide silanes; the presence of a silicon peak in the XPS spectra was further indication that the conjugation was successful.

Table 2 MALDI-MS characterization of synthesized molecules. Some of the peptide silanes appear to have undergone partial or complete hydrolysis of the APTMS methyl groups, as evidenced by the expected *m/z* ratio being lower by a factor of 15 amu. There are artifacts of peptides still containing protective side chain groups, indicating slight impurities in the samples, which was not a concern in the scope of this study

Sample	Nominal molecular mass/g mol ⁻¹	<i>m/z</i> Reported
NID peptide silane	1421	1391.44 ^b (M ⁺ , 18%), 1384.67 (29), 1286.31 (45), 1253.43 (35), 1248.37 (78), 1232.42 (67), 1222.37 (34), 691.22 (27), 643.99 (36), 622.17 ^a (100), 606.20 (68), 568.06 (40), 542.20 (62), 525.17 (32)
NID free peptide	1216	1348.40 ^c (10%), 1318.29 ^c (11), 1260.25 (65), 1244.28 (42), 1222.31 ^a (100), 1206.33 ^c (65), 643.93 (66), 622.14 (66), 606.16 (46), 587.04 (20), 542.17 (17)
RGD peptide silane	1559	1545.37 ^b (M ⁺ , 17%), 1433.38 (28), 1394.37 (22), 1348.32 (55), 1322.35 ^a (100), 1293.33 (77), 1114.27 (23), 915.24 (22), 859.19 (38), 772.20 (36), 702.15 (50), 643.86 (30)
RGD free peptide	1354	1362.43 ^c (25%), 1349.51 ^c (M ⁺ , 36), 1322.41 ^a , 1293.38, 1251.35 (25), 1206.36 (17), 1179.62 (18), 968.28 (12), 802.21 (21), 702.18 (13), 643.05 (11)
KDI peptide silane	1621	1598.46 ^b (M ⁺ , 16%), 1553.65 (19), 1504.69 (17), 1448.59 (21), 1423.63 (23), 1410.65 ^a (100), 1384.68 (60), 1291.80 (22), 1199.51 (13), 971.47 (11), 794.48 (10), 696.27 (14), 571.22 (12)
KDI free peptide	1416	1480.69 ^c (11%), 1460.62 ^c (12), 1420.61 (30), 1406.69 (M+, 17), 1384.73 ^a (100), 1327.69 (27), 1143.58 (5), 971.51 (5), 697.13 (4), 644.00 (3)
YIG peptide silane	1382	1449.67 ^c (17%), 1383.31 (M ⁺ , 14), 1258.52 (19), 1231.48 (23), 1159.41 (32), 1089.42 ^a (100), 1075.48 (48), 1063.44 (49), 919.38 (46), 854.42 (24), 643.22 (12), 602.29 (14), 586.27 (18)
YIG free peptide	1177	1205.48 ^c (13%), 1175.89 (M ⁺ , 9), 1159.38 (53), 1093.43 (12), 1085.38 (12), 1063.41 ^a (100), 935.35 (13), 917.64 (15), 905.37 (8), 903.34 (13), 805.29 (30), 658.32 (15), 630.27 (17), 602.24 (10)

^a Highest intensity. ^b Partial hydrolysis. ^c Small peak—likely artifact of remaining protective groups.

Table 3 XPS survey spectra elemental percentages. Each surface bound peptide silane and free peptide silane were analyzed using XPS. The atomic percentages were derived using the survey scans collected at 160 eV. The carbon signal was further scanned at 20 eV to support elimination of organic noise from the spectral data. Organic C–C bonds were mathematically resolved from the peptides of interest through mathematical comparison to the free peptide silane, as described by Jedlicka *et al.*³¹ Following this organic elimination, the nitrogen to carbon ratios between the peptides and peptide silanes were compared to those ratios derived from structural analysis (*i.e.*, a count of each atom present in the proposed structure)

Sample	C 1s (%)	F 1s (%)	N 1s (%)	O 1s (%)	Si 2p (%)	Na 1s (%)	P 2p (%)	Molecular C 1s from peptide (%)	N/C ratio	
KDI surface silane	17.72	3.02	3.02	53.10	19.74	2.68	0.72	11.09	0.27	XPS
KDI silane	58.28	5.55	13.78	20.70	2.47			51.76	0.26	Ideal
NID surface silane	10.16	2.34	1.31	61.21	22.20	2.18	0.60	4.54	0.27	XPS
NID silane	52.52	7.92	14.11	22.62	2.84			42.32	0.28	Ideal
RGD surface silane	9.40	0.38	0.67	60.78	28.12	0.52	0.13	3.53	0.29	XPS
RGD silane	53.37	4.55	14.59	25.44	2.38	0.60		47.53	0.29	Ideal
YIG surface silane	13.61	0.95	1.40	58.53	24.82	0.70	0.11	5.45	0.31	XPS
YIG silane	56.57	7.75	10.54	19.03	2.77	0.02		38.38	0.31	Ideal

X-Ray photoelectron spectroscopy

To confirm the presence of the peptides at the surface of the peptide silane silica films, X-ray photoelectron spectroscopy (XPS) was employed to analyze the atomic composition of the peptide silane thin films. Thin films were prepared as described below, using a final concentration of 0.1 mol% peptide silane to TMOS derived silica. This ratio, while significantly higher than many of the potential biological ratios that will be used in the future, represents a quantity that is easily detected by XPS. Future work will include calibration curve analysis to determine the lowest surface relevant concentration.

XPS spectra were analyzed and deconvoluted to yield atomic percentages present on the surface of the materials. Organic contamination was eliminated from the sample spectrum through mathematical means described elsewhere.³¹ The atomic percentages are presented in Table 3. The XPS data reveal the presence of carbon and nitrogen species on the SiO₂ surface. To confirm that the carbon and nitrogen peaks were from the peptides, the ratio of N : C was compared to the ideal N : C derived from the expected structure. The structural N : C was obtained by enumerating the carbon and nitrogen atoms in the expected molecular structure. These ratios are within reasonable limits of the ideal N : C, providing reasonable confirmation that the organic species present on the surface of the peptide-derived silica thin films is from the incorporated peptide.

The correlation between the ideal N : C based on structural information and the experimental N : C of the non-silicon bound peptide silanes can also help confirm that the peptide synthesis was successful and that there are not any significant additions or deletions in the peptide sequence. While it is evident from many of the contaminating species in the spectra, such as sodium and fluoride, that the peptide silanes are not of a purity normally required for peptide studies, the purity of the ormosil surfaces is enhanced through multiple washes of the resultant thin films. This eliminates unwanted atomic species and leftover organics from the synthesis reaction, which could

potentially interact negatively with cells. Each of the contaminating species can be attributed directly to synthesis and purification agents; specifically, fluorine byproducts are associated with trifluoroacetic acid cleavage.

In addition to analysis of the surface bound peptide silanes, XPS analysis was performed on the free peptides and free APTMS conjugated peptides (peptide silanes). The atomic percentages are presented for the RGD peptide in Table 4. The carbon, nitrogen, and oxygen profiles of the free peptides and peptide silanes are similar between the samples, with the primary differences occurring in the oxygen and silicon peaks. Of significant importance, the silicon peak is apparent in the silane conjugated peptides, at 2.38%, while there appears to be only background contaminant silicon in the peptide, with a spectral percentage of 0.01%. In addition, the oxygen percentage is considerably larger in the peptide silane spectrum (+5%), which may be attributed to the silane-derived methoxy groups that may still be attached to the molecule. This comparison between the free peptides and peptide silanes provides additional confirmation of the successful conjugation between the APTMS molecule and peptide chain.

The XPS data indicate the availability of the peptide on the surface of the silica thin films. In addition, they serve as a confirmation of the successful silane conjugation on the amine

Table 4 XPS elemental comparison between peptide silane and free peptide. For comparative purposes, the RGD peptide silane and free peptide were subject to a 160 eV survey scan. The elemental percentages were compared to confirm the successful conjugation of the APTMS molecule to the peptide chain. The data indicate that the elemental percentages are in close agreement between the silane-conjugated and free peptide, with the exception of the silicon atom. This appears in only the silane survey scan. These data also confirm that the silicon is not from potential extraneous contamination

	C 1s (%)	F 1s (%)	N 1s (%)	O 1s (%)	Si 2p (%)	Na 1s (%)
RGD silane	53.37	4.55	14.59	25.44	2.38	0.60
RGD peptide	58.19	4.91	15.56	20.06	0.01	0.01

terminus of the peptide. Given the bulky nature of these molecules, the surface nanotopography may be altered by the addition of peptide quantities at biologically relevant concentrations. To test this theory, AFM was employed to examine the nanotopographical and phase interactions of the thin film ormosils.

Surface features of the peptide ormosils

Previous studies by our lab indicate that the nanostructure of silica sol-gel surfaces plays a fundamental role in neuronal adhesion and survival properties.²³ Specifically, thin-film sol-gel morphology, with height features ranging between 25–100 nm, supports PC12 neuronal adhesion. In contrast, bulk silica monoliths, with features ranging from 100–250 nm, are non-permissive to PC12 neuron adhesion. These adhesion profiles have been determined to be associated with electrostatic and topography-induced patterns of ECM protein unfolding on the various surfaces. The presence of ECM peptides in the materials, however, will likely reduce or alter the effects of nanotopography by providing specific cell binding sites at the surface. To determine the nanotopography of the peptide silane material surfaces, AFM images were collected of thin films produced from each of the four peptide silane precursors at mole percentages used in the cell studies. These images principally serve to confirm that the addition of bulky peptide molecules at biologically relevant ratios does not significantly alter the thin film features outside of the range of native thin films. Any changes in cell function on the peptide ormosils are therefore likely due to the peptides themselves and not secondary changes in surface features. Fig. 2 presents representative images of the thin films.

The NID and KDI materials were prepared at a higher mole percentages compared to the basic cell adhesion peptides YIG and RGD. Both the NID and KDI materials have well defined surface features in the range of 50–75 nm. In addition, a small amount of noise resulted from the tip sticking to the surface indicating tip-material interactions were present. This interaction is not observed in unmodified TMOS films³² and is likely due to the presence of the peptide.

YIG and RGD were used at extremely low concentrations (0.0025 mol%) based on biological function. The resulting films lack defined features and appear similar to unmodified TMOS derived films.²³ These AFM images, therefore, indicate that surface nanotopography is likely a function of the concentration of peptide at the surface.

The nanotopography of the thin film materials is consistent with the morphology observed in TMOS thin films, which are capable of supporting neuronal adhesion. Therefore, it is reasonable to assume that the peptide modified silica films will be able to support cellular adhesion. The larger features apparent on the NID and KDI films are approaching the feature size of bulk gel materials, however, the incorporation of the peptide derived integrin ligands should eliminate any undesired effects on cell adhesion due to feature size by supplying specific cell binding sites. To examine this potential of the materials to support neuronal cells, P19 cells were used as a cellular model.

Cellular response of pluripotent P19 cells

P19 cells are an established model for studying neuronal differentiation and were selected for demonstrating the biological functionality of the peptide ormosils. Established

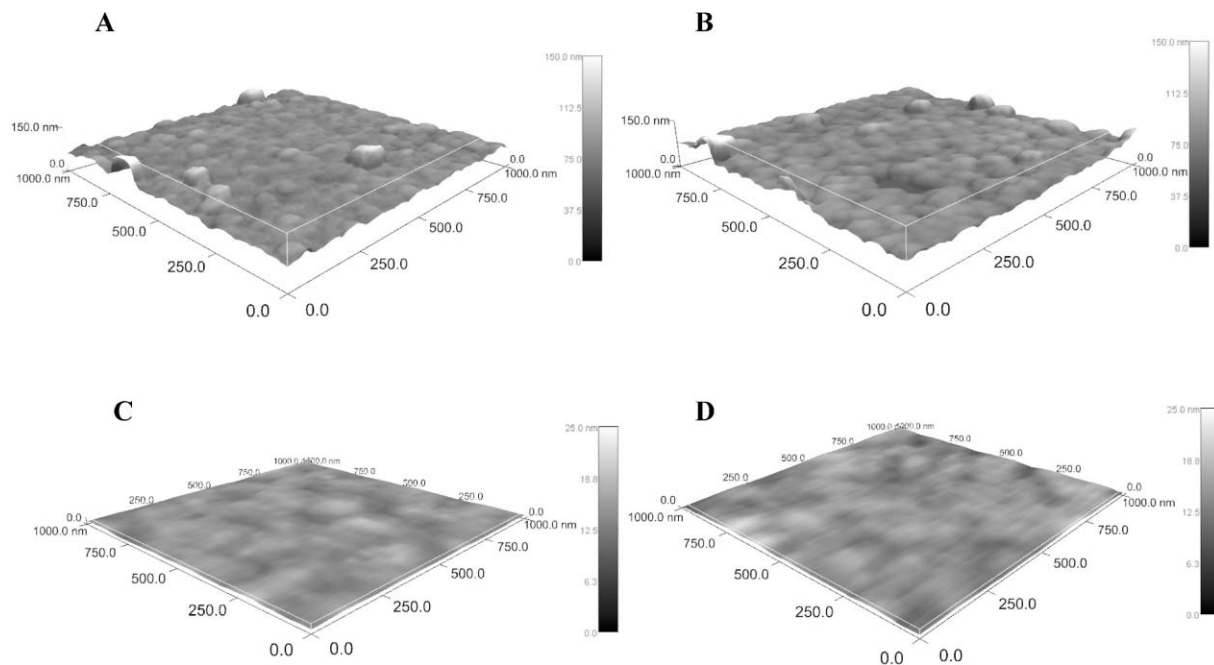


Fig. 2 Surface topography of peptide films. AFM height images of thin films produced from peptide silane and TMOS precursors. (A) NID peptide silane (0.01% in TMOS sol-gel), (B) KDI peptide silane (0.01% in TMOS sol-gel), (C) RGD peptide silane (0.0025% in TMOS sol-gel), (D) YIG peptide silane (0.0025% in TMOS sol-gel). The concentrations chosen for imaging correlate to the final concentrations (mol%) used in the cell studies.

by McBurney in 1982,^{33,34} P19 cells are a pluripotent embryonic carcinoma cell line with many features of embryonic stem cells.³⁵ When exposed to retinoic acid (RA) and allowed to aggregate, P19 cells can differentiate into fibroblast-like, glial, and neuronal cells.^{36–39} The ratio of cell types varies with extracellular environment conditions in the culture. The resulting neurons can mature to form both inhibitory and excitatory synaptic connections.³⁶

We hypothesized that the peptide ligands in the material composition would alter the differentiated cell composition and neuronal morphology after retinoic acid treatment. Due to the dramatic differences in the morphology and biochemical characterization of neurons compared to astrocytes and fibroblasts, these cell population compositional changes should be easily observed by microscopy and immunofluorescent techniques. After retinoic acid treatment, cells were plated on thin films containing a combination of the basic adhesion peptides, RGD and YIG, as well as on films containing the three peptides RGD/YIG/NID (see Table 5). The first composition was chosen to determine if the simple addition of two commonly used adhesion peptides to the surfaces of the thin film materials would enhance the utility of silica thin films as a cell culture substrate. The second material was chosen to explore the potential effects of adding a peptide known to play a role in extracellular patterning and basement membrane formation (NID), creating a more “rich” extracellular environment. The final peptide discussed in this paper (KDI) was not used in cell studies, but will be explored in future work. The primary function of the KDI peptide is neuronal pathfinding and could potentially be useful in spatial cell direction.

Based on developmental research, it is well known that many extracellular matrix proteins, specifically fibronectin, only appear in limited amounts during neural stem cell proliferation, differentiation, and migration.⁴⁰ Therefore, the fibronectin RGD group was used at a very low molar ratio. The YIG group, known as a neuronal cell adhesion molecule, was also limited in molar ratio for the purposes of this study. As protein quantification in the absolute sense is somewhat elusive, these ratios represent a combination of developmental ratios, primarily based on whole protein analysis, and quantities used in existing peptide-modified biomaterial work.

Fig. 3 shows cells plated on the peptide materials compared to cells on the unmodified TMOS derived thin film and on a collagen coated tissue culture plate control. The cells were maintained on the materials in α -MEM supplemented with 1% FBS to ensure that the cells were interacting with the peptide

Table 5 Experimental materials for cell studies. Three peptide silanes in two combinations were explored to explore the potential utility of the peptide silane thin films. The peptide silanes were incorporated into the silica thin films using the ratios shown. These materials were compared to standard 30% TMOS sol-gel derived silica thin films and collagen coated tissue culture plastic

	TMOS sol	Peptide silane	Mol% added
Adhesion peptides	30%	RGD	0.025%
		YIG	0.025%
Adhesion + BM peptides	30%	RGD	0.025%
		YIG	0.025%
		NID	0.100%

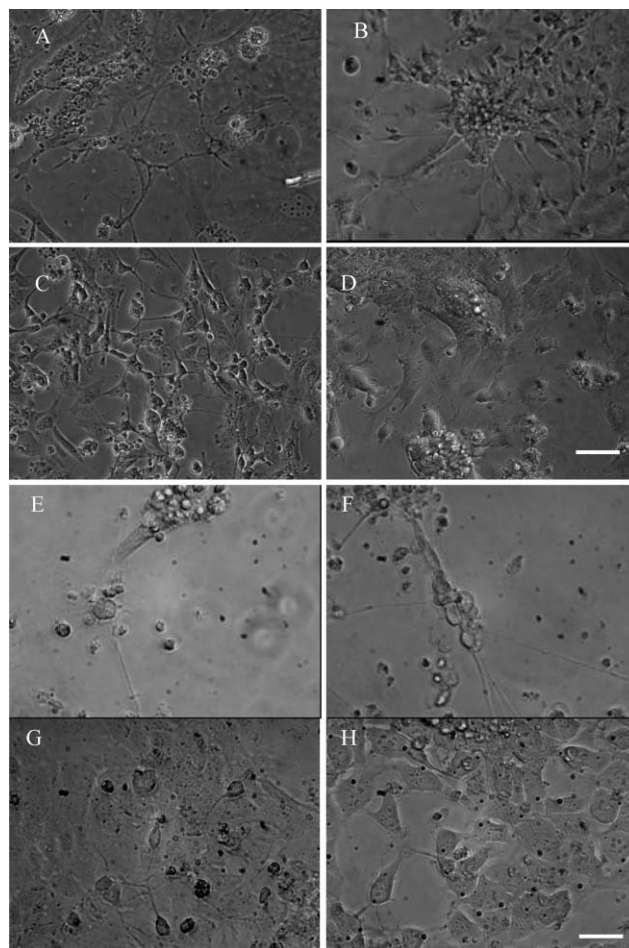


Fig. 3 Analysis of cell morphology. P19 cells imaged 10 days after RA induction on peptide surfaces compared to unmodified film control and collagen-coated tissue culture control. A–D are images taken at 200 \times (scale bar = 100 μ m). A. RGD/YIG sol-gel films; B. RGD/YIG/NID sol-gel films; C. collagen-coated tissue culture control; D. TMOS derived silica films. E–H are images taken at 400 \times (scale bar = 50 μ m). E. RGD/YIG sol-gel films; F. RGD/YIG/NID sol-gel films; G. collagen-coated tissue culture control; H. TMOS derived silica thin films. The peptide modified silica thin films appear to enhance the maturity of the adherent neurons over the collagen control and native silica films. The native silica films will support adhesion of the differentiated P19 cells, however, there appears to be a reduced number of neurons, and the neuronal morphology is immature. Thus, the peptide modifications to the silica films appear to enhance the differentiation of the P19 cell population.

materials and not a layer of serum proteins. This treatment has also been shown to increase the proportion of neuronal cells in the differentiated population,³⁸ due to the starvation of non-neuronal and undifferentiated cells. The cellular response to the materials was qualitatively analyzed using standard morphological observation. The unmodified TMOS films result in few neurons (Fig. 3C). Of noteworthy importance, in the low serum environment, the cells only rarely migrated out of the plated aggregates on the TMOS derived silica. In contrast, the RGD/YIG films (Fig. 3A) appear to enhance the neuronal morphology of the cells over standard TMOS derived silica thin films. When the NID peptide, known to facilitate extracellular matrix interactions, was included, an increase in

neuronal processes per field of view was observed. A network of long cellular processes forms on both peptide modified materials. In addition, both of these peptide ormosils appear to support a wide variety of morphologically-distinct cell types, while the collagen control seems to support a larger proportion of neuronal cells. As these observations are purely based on cell morphology, a quantitative analysis of cell type was conducted.

To analyze the cell type and confirm the morphological observations, several assays were performed. First, confocal analysis of β -tubulin III was performed to examine the neurite patterns of the adherent neuronal cells (Fig. 4). The confocal images indicate that while each material type does support neuronal cells, the neurite processes on each of the material types are altered in agreement with the initial morphological observations. On the collagen-coated tissue culture control, there are several β -tubulin positive cells in each view, however, the neurite processes of these cells are relatively short. In addition, the lack of nuclei not associated with the neuronal cells demonstrates a lack of supporting glial cells. In contrast, the RGD/YIG and RGD/YIG/NID peptide silane thin films supported a variety of cells, shown by the density of nuclear staining. The neurite processes on these two material types are also much longer than the collagen control. The RGD/YIG/NID peptide silane films also seemed to support more neurite processes per field (Fig. 4B). Overall, the peptide-modified silica films appear to enhance the neuronal maturation of the P19 cells over the collagen control surfaces and native silica films.

As an additional confirmation of the morphological differences of adherent cells, neurite length was quantified using the NeuronJ plugin of ImageJ.⁴¹ Neurites were traced from the cell body and quantified based on pixel conversion to micrometers. At least 5 images were analyzed per experiment, with at least 10 neurite traces performed per image. These data are presented in Fig. 5. The peptide silane materials supported longer neurite processes, which is likely due to the density of glial cells enhancing the maturation of the adherent neurons. The RGD/YIG, surprisingly, supported longer neurites than the RGD/YIG/NID combination, although the RGD/YIG/NID combination did appear to support more neurite processes per field. The collagen control surfaces do sustain the neuronal population, however, based on neurite length, it can be reasonably deduced that the neuronal cells are less mature than those associated with the peptide ormosil materials. The TMOS derived silica films, as expected, supported the shortest processes.

As an initial examination of the potential of the materials to modulate cell type, FACS analysis was performed to quantify the percentage of neuronal and astrocytic cells in the culture population. Neuronal cells were labeled with AlexaFluor 488 conjugated β -tubulin III, and astrocytic cells labeled with Cy3 conjugated GFAP. These data are presented in Table 6. The collagen control, as expected, supports the largest percentage of neuronal cells and a smaller percentage of astrocytic “support” cells over the peptide modified silica films. The TMOS derived silica supports very few neurons (0.875%), as

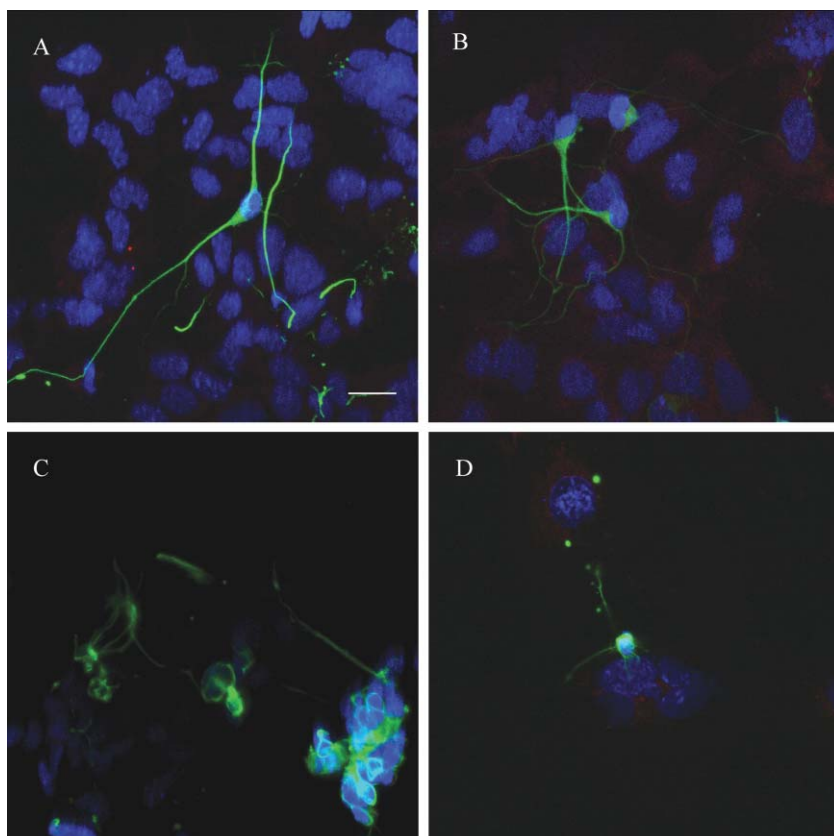


Fig. 4 Confocal immunofluorescent expression of Tuj1. *In situ* immunofluorescent analysis was performed to analyze neuronal lineages and observe neurite patterns between materials. (A) RGD/YIG; (B) RGD/YIG/NID; (C) collagen; (D) TMOS derived silica (scale bar = 75 μ m).

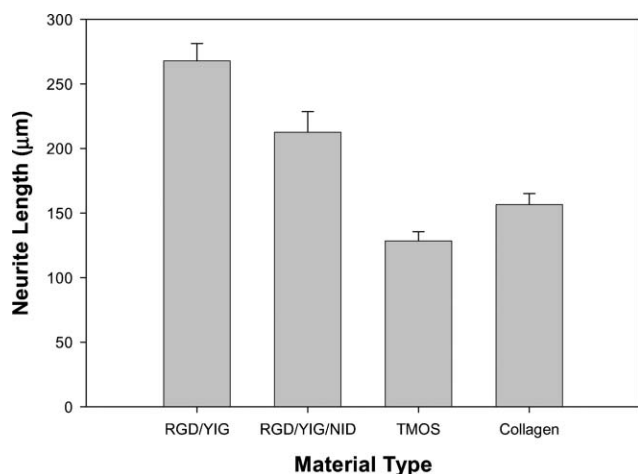


Fig. 5 Neurite length analysis. Images were collected of live cells at 8–10 days after seeding post-RA induction. The images were analyzed for neurite length using the NeuronJ plugin for ImageJ. Neurites were traced from the cell body to the terminal end of the primary neurite. Secondary neurites were observed but not quantified in this analysis. The length of the neurites was compared using a student's t-test to the collagen control, and the neurite lengths were found to be statistically larger than that of the control cells ($\alpha < 0.05$).

Table 6 Immunopositive cell type analysis. Material-exposed P19 embryonic carcinoma cells were grown on the described material types for 8–10 days. Cells were then removed from the materials and subjected to immunocytochemical protocols and FACS analysis. The percentage of cells positive for the various antibodies (GFAP: astrocytic cells, Tuj1: neuronal cells) are presented. The numbers in parentheses are the standard error across the experiments

	TMOS silica	RGD/YIG	RGD/YIG/NID	Collagen control
Tuj1+ ^a	0.875 (0.325)	2.86 (0.35)	5.325 (0.48)	15.58 (0.82)
GFAP+	9.625 (1.57)	9.75 (2.46)	13.725 (1.23) ^a	6.9 (0.66)

^a $\alpha < 0.05$.

well a population of astrocytic cells. Considering the infrequency with which the cells migrated out of aggregates on the TMOS derived silica, these data are reasonable. The peptide materials, based on cell type analysis, appear to have a significant effect on the cell population. The RGD/YIG “adhesion” material appears to promote a significantly smaller population of neuronal cells than the collagen control and the RGD/YIG/NID composition. In addition, the RGD/YIG/NID composition espouses a larger number of astrocytic cells, which may enhance the ability of neurons to develop, survive, and ultimately mature. Overall, the cell population analysis appears to correlate with the neurite length quantification and confocal analysis of the differentiated P19 cells.

The NID peptide is known to be involved in a variety of cellular signals. While we cannot be certain what pathways are being modulated, it is evident that the NID peptide does enhance the neuronal population in terms of neuronal percentages over the RGD/YIG material. The numerical count of neurons is less than that on the collagen control surfaces. In addition, given the increased length of neurites and formation of a network of processes on the RGD/YIG/NID surfaces, it is possible that the neurons have reached functional maturity.

The selected peptides used in this study have all been drawn from known integrin interactions in the developing vertebrate nervous system. Integrins are the major class of receptors utilized by cells to interact with ECM protein ligands. Upon ligand binding, integrins cluster on the cell surface at sites termed focal adhesions, leading to the assembly of intracellular multiprotein complexes associated with the cytoskeleton.⁴² Focal adhesions, beyond acting as structural links between the ECM and cytoskeleton, are sites of signal transduction from the ECM. The manipulation of P19 population phenotype demonstrates that the incorporated peptides are available to the receptors at the cell surface and the peptide precursors are able to impart biological functionality into the sol-gel thin films.

Conclusion

We have demonstrated a method for the synthesis of chemically conjugated peptides to silane precursors. These precursors can then be added at particular mole percentages to standard TMOS derived silica thin films during condensation to improve the biological compatibility and ultimately neuronal differentiation patterns of P19 embryonic carcinoma cells. Through the use of selected cellular interactions, we have shown that the identity and maturity of the experimental cells can be modified.

Previous work by many groups have focused on the facilitation of neuronal growth through the use of biomaterials modified with extracellular matrix (ECM) components such as immunoglobulin, vitronectin, fibronectin, and laminin. These studies indicated that cellular migration, axon growth and guidance, and neuronal differentiation can be enhanced through the incorporation of proteins and peptides that mimic the ECM. Our study has improved upon previous peptide work by integrating multiple ECM components to enhance the neuronal phenotype of the pluripotent cell type. We have demonstrated the flexibility of the method by characterizing films produced from four different peptides as well as an ability to combine multiple peptides in one material. In addition, the sol-gel method has many commercial advantages and this new “one pot” method using peptide silanes will enable a simple way to create a wide range of biologically active films.

Experimental

Peptide silane synthesis

Peptides were synthesized using standard Fmoc solid state synthesis on an Intavis Multi-Pep synthesizer. Wang resin was preloaded with the C-terminal amino acid using dimethylaminopyridine (DMAP) catalyzed esterification.⁴³ Protected amino acids were added to the growing peptide chain with the activating reagent 2-(1*H*-benzotriazol-1-yl)-1,1,3,3-tetramethyluronium hexafluorophosphate (HBTU).⁴⁴ Upon the addition of the N-terminal amino acid, the Fmoc group was removed under standard 20% piperidine deprotection conditions. 1,1'-Carbonyldiimidazole (CDI) (0.4 M in methylene chloride) was then added to the peptide chain under inert gas to activate the N-terminus amino group. Following activation

and washing, 0.4 M aminopropyltrimethoxysilane (APTMS) in methylene chloride was attached to the activated N-terminal, forming a covalent linkage between the peptide N-terminal amine and the APTMS with a C=O spacer. After cleaving all side chain protective groups, the peptide silanes were ether precipitated and crudely purified prior to use. MALDI-mass spectrometry analysis was used as confirmation efficient silane coupling and expected m/z ratio.

Thin film materials synthesis

The peptide silanes were dissolved in a 50 μL drop of dimethyl sulfoxide (DMSO), suspended in buffer and added in appropriate molar ratios (see Table 4 and Fig. 2) to 30% tetramethoxysilane (TMOS) acid-hydrolyzed sol in sterile 0.02 M pH 7.4 phosphate buffer, with 10% of the final volume of methanol added to slow gelation. Cleaned glass 8 mm glass coverslips (WPI) were dip-coated into the mixture at a constant rate (35 mm s^{-1}) to create films of approximately 100 nm in thickness. Films were briefly disinfected in isopropanol or ethanol prior to use and then soaked in buffer for at least 48 h to remove any synthesis byproducts and to stabilize the peptides. The peptide silanes contain short peptide chains (6–14 mer), and were designed to limit secondary structure formation on the resin, thus we did not anticipate or observe significant degradation or denaturation under the mild alcohol conditions used above. For cell culture purposes, the thin-film materials were also sterilized under a UV lamp for a minimum of 16 hours.

X-Ray photoelectron spectroscopy

XPS data were obtained by a Kratos Ultra DLD spectrometer equipped with a monochromatic Al $K\alpha$ radiation ($h\nu = 1486.58$ eV). A fixed analyzer pass energy of 160 eV was used to collect survey spectra, and a pass energy of 20 eV was used to collect narrow region spectra. Atomic percentages from the spectral data were determined as discussed by Jedlicka *et al.*³¹

Atomic force microscopy

Peptide TMOS thin films were imaged in buffer using a fluid cell and a closed-loop atomic force microscope (Asylum Research) operating in AC mode at a scan rate of 1 Hz. The AFM was used to determine the nanotopographical characteristics. The thin films were prepared using filtered materials (0.2 μm pore size) as described and transferred to a sterile hood. After preparation, materials were quickly attached to a glass window of the fluid cell with waterproof, fast setting resin-based adhesive. After allowing 15–30 s to adhere, the samples then were placed in gel purified pH 7.4 phosphate buffer. The gels were rinsed and transferred to clean buffer, to prevent any resin byproducts from interfering with the gel structure. Samples were sealed into the fluid cell, immediately covered with the phosphate buffer, and imaged. For all imaging experiments, 60 μm long SiN bio-lever probes (Olympus) with a 0.027 N m^{-1} spring constant were used and Z-series, phase, and amplitude traces and retraces were collected and compared. The probe tips had an approximate radius of curvature of 40 nm. The 512 \times 512 pixel images were

scanned at a rate of 1 Hz. The images were flattened under a first order correction and analyzed for height distributions using IgorPro software.

Cell culture

P19 embryonic carcinoma cells were obtained from ATCC (CRL-1825). Cells were routinely cultured in α -MEM (Mediatech) supplemented with 7.5% bovine calf serum (BCS) and 2.5% fetal bovine serum (FBS) (Hyclone). Cells were passaged at 75% confluency or every four days using trypsin EDTA (Hyclone). To induce neuronal differentiation, cells were exposed to 5×10^{-7} M all-*trans* retinoic acid (Sigma Aldrich) in α -MEM medium supplemented with 0.5% FBS in 10 cm bacteriological grade petri dishes (Falcon) for 5 days. Post-induction, cells were plated on UV-sterilized 8 mm peptide silane thin films, TMOS thin films, and control tissue culture dishes (Corning) coated with 0.5 mg mL^{-1} rat tail collagen (Becton Dickinson) at a density of 40 000 cell cm^{-2} . Differentiated cells were fed every two days using a low serum version of the standard media formulation for maintenance of P19 cells. Specifically, the serum concentration was reduced to 1% FBS in α -MEM. Cells were imaged daily to track morphological changes with a Nikon inverted T100 microscope and attached CoolSnap camera. Cell morphology was quantified from the brightfield images using the NeuronJ plugin of ImageJ. Primary neurites were traced from the cell body and converted to micrometers from pixel counts.

Cells were assessed using both flow cytometry and immunofluorescence quantification. Flow cytometrical cell type analysis of the differentiated cell populations was acquired at 8–10 days post-seeding. Cells were detached from the materials using trypsin-EDTA. Following detachment, cells were resuspended in one part 50% FBS in PBS (phosphate buffered saline) (pH 7.4), and fixed with three parts ice-cold 70% ethanol overnight at 4 $^{\circ}\text{C}$. Fixed cells were then permeabilized for 10 min in PBS (pH 7.4) with 0.1% Triton X-100, 1% bovine serum albumin and 1% sodium azide (PBS-T). Following permeabilization, cells were blocked for one hour at room temperature using PBS-T supplemented with 10% normal goat serum. Alexa 488 conjugated antibody to beta-tubulin III (Tuj1, Covance) and Cy3 conjugated antibody to glial fibrillary acidic protein (GFAP, Sigma) were used to detect neurons and astrocytes, respectively. The primary antibodies were added to the blocked cells in PBS-T supplemented with 1% normal goat serum (NGS), and the cells gently agitated overnight at 4 $^{\circ}\text{C}$, followed by washing three times in PBS-T. The cells were subsequently washed three times and analyzed using a Beckman Coulter Altra Cell Sorter. The percentage of cells positive for the immunochemical markers was averaged over at least four independent cell populations. A Student's t-test was performed to determine significance of the population differences ($\alpha < 0.05$).

In situ immunofluorescence staining and confocal analysis was also performed to confirm the flow cytometric data and brightfield morphological analysis. Briefly, cells were fixed *in situ* using 4% paraformaldehyde for 15 min, followed by washing in PBS-T and permeabilization with 0.1% Triton X-100. Cells were blocked in PBS-T with 10% normal goat

serum. Antibodies identical to the flow cytometric protocols were added to the plates following the timing as discussed above. After the final washing, the cells were analyzed using a Bio-Rad Radiance Multiphoton confocal microscope.

Acknowledgements

The authors gratefully acknowledge Dr Don Bergstrom and Dr Jianjie Huang of the Bindley Bioscience Center Biomolecular Synthesis Labs for guidance and use of the peptide synthesizer. Karl Wood of the Purdue Mass Spectrometry facility is acknowledged for operation of the MALDI-MS. In addition, the authors acknowledge J. Paul Robinson, Jennie Sturgis, Kathy Ragheb and Cheryl Holdman of the Purdue University Cytometry Labs for use and operation of the Altra Cell Sorter and multiphoton confocal microscope. Craig Barcus of the Physiological Sensing Facility is acknowledged for his assistance in material preparation of the thin films. SSJ was supported by the Purdue Research Foundation. We also gratefully acknowledge the support of the Citizens United for Research for Epilepsy through the Christopher Donalty Interdisciplinary Research Award.

References

- 1 F. Doetsch, *Curr. Opin. Genetics Dev.*, 2003, **13**(5), 543–550.
- 2 L. S. Campos, *BioEssays*, 2005, **27**(7), 698–707.
- 3 A. S. Goldstein and P. A. DiMilla, *J. Biomed. Mater. Res.*, 2002, **59**(4), 665–675.
- 4 M. A. Biesalski, A. Knaebel, R. Tu and M. Tirrell, *Biomaterials*, 2006, **27**(8), 1259–1269.
- 5 C. Briones, E. Mateo-Marti, C. Gomez-Navarro, V. Parro, E. Roman and J. A. Martin-Gago, *Phys. Rev. Lett.*, 2004, **93**(20).
- 6 Y. Z. Feng and M. Mrksich, *Biochemistry*, 2004, **43**(50), 15811–15821.
- 7 E. Mateo-Marti, C. Briones, E. Roman, E. Briand, C. M. Pradier and J. A. Martin-Gago, *Langmuir*, 2005, **21**(21), 9510–9517.
- 8 N. Patel, R. Padera, G. H. W. Sanders, S. M. Cannizzaro, M. C. Davies, R. Langer, C. J. Roberts, S. J. B. Tendler, P. M. Williams and K. M. Shakesheff, *FASEB J.*, 1998, **12**(14), 1447–1454.
- 9 T. A. Petrie, J. R. Capadona, C. D. Reyes and A. J. Garcia, *Biomaterials*, 2006, **27**(31), 5459–5470.
- 10 X. G. Wen, R. W. Linton, F. Formaggio, C. Toniolo and E. T. Samulski, *J. Phys. Chem. A*, 2004, **108**(45), 9673–9681.
- 11 C. J. Wilson, R. E. Clegg, D. I. Leavesley and M. J. Percy, *Tissue Eng.*, 2005, **11**(1–2), 1–18.
- 12 K. Wilson, S. J. Stuart, A. Garcia and R. A. Latour, *J. Biomed. Mater. Res., Part A*, 2004, **69A**(4), 686–698.
- 13 C. Calonder, H. W. T. Matthew and P. R. Van Tassel, *J. Biomed. Mater. Res., Part A*, 2005, **75A**(2), 316–323.
- 14 D. Avnir, S. Braun, O. Lev and M. Ottolenghi, *Chem. Mater.*, 1994, **6**(10), 1605–1614.
- 15 T. R. Besanger, B. Easwaramoorthy and J. D. Brennan, *Anal. Chem.*, 2004, **76**(21), 6470–6475.
- 16 T. Besanger, Y. Zhang and J. D. Brennan, *J. Phys. Chem. B*, 2002, **106**, 10535–10542.
- 17 J. X. Zhao, S. S. Jedlicka, J. D. Lannu, A. K. Bhunia and J. L. Rickus, *Biotechnol. Prog.*, 2006, **22**(1), 32–37.
- 18 T. Nguyen and Z. Rosenzweig, *Abstr. Pap. Am. Chem. Soc.*, 1999, **218**(1–2), 284.
- 19 S. Chia, J. Urano, F. Tamanoi, B. Dunn and J. I. Zink, *J. Am. Chem. Soc.*, 2000, **122**(27), 6488–6489.
- 20 J. F. T. Conroy, M. E. Power, J. Martin, B. Earp, B. Hosticka, C. E. Daitch and P. M. Norris, *J. Sol–Gel Sci. Technol.*, 2000, **18**, 269–283.
- 21 J. A. Cruz-Aguado, Y. Chen, Z. Zhang, N. H. Elowe, M. A. Brook and J. D. Brennan, *J. Am. Chem. Soc.*, 2004, **126**(22), 6878–6879.
- 22 P. Szaniszlo, W. A. Rose, N. Wang, L. M. Reece, T. V. Tsulaia, E. G. Hanania, C. J. Elferink and J. F. Leary, *Cytometry, Part A*, 2006, **69A**(7), 641–651.
- 23 S. S. Jedlicka, J. L. McKenzie, S. J. Leavesley, K. M. Little, T. J. Webster, J. P. Robinson, D. E. Nivens and J. L. Rickus, *J. Mater. Chem.*, 2006, **16**(31), 3221–3230.
- 24 C. Zolkov, D. Avnir and R. Armon, *J. Mater. Chem.*, 2004, **14**, 2200–2205.
- 25 Z. Zhang, R. Yoo, M. Wells, T. P. Beebe, R. Biran and P. Tresco, *Biomaterials*, 2005, **26**(1), 47–61.
- 26 E. Ruoslahti, *Glycobiology*, 1996, **6**(5), 489–492.
- 27 J. P. Ranieri, R. Bellamkonda, E. J. Bekos, T. G. Vargo, J. A. Gardella and P. Aebischer, *J. Biomed. Mater. Res.*, 1995, **29**(6), 779–785.
- 28 P. Liesi, T. Laatikainen and J. M. Wright, *J. Neurosci. Res.*, 2001, **66**(6), 1047–1053.
- 29 J. Garwood, F. Rigato, N. Heck and A. Faissner, *Restorative Neurol. Neurosci.*, 2001, **19**(1–2), 51–64.
- 30 E. Garcion, A. Halilagic, A. Faissner and C. ffrench-Constant, *Development*, 2004, **131**(14), 3423–3432.
- 31 S. S. Jedlicka, J. L. Rickus and D. Y. Zemlyanov, Surface Analysis by X-ray Photoelectron Spectroscopy of Sol–Gel Silica Modified with Covalently Bound Peptides, *J. Phys. Chem. B*, 2007, **111**(40), 11850–11857.
- 32 S. S. Jedlicka, S. J. Leavesley, K. M. Little, J. P. Robinson, D. E. Nivens and J. L. Rickus, in *Interactions Between Chemical Functionality and Nanoscale Surface Topography Impact Fibronectin Conformation and Neuronal Differentiation on Model Sol–gel Silica Substrates*, MRS Fall Meeting, Boston, 2006, submitted.
- 33 M. McBurney and B. Rogers, *Dev. Biol.*, 1982, **89**(2), 503–508.
- 34 M. W. McBurney, *Int. J. Dev. Biol.*, 1993, **37**(1), 135–140.
- 35 D. I. Gottlieb, *Annu. Rev. Neurosci.*, 2002, **25**, 381–407.
- 36 P. A. MacPherson, S. Jones, P. A. Pawson, K. C. Marshall and M. W. McBurney, *Neuroscience*, 1997, **80**(2), 487–499.
- 37 D. S. K. Magnuson, D. J. Morassutti, M. W. McBurney and K. C. Marshall, *Dev. Brain Res.*, 1995, **90**(1–2), 141–150.
- 38 W. A. Staines, J. Craig, K. Reuhl and M. W. McBurney, *Neuroscience*, 1996, **71**(3), 845–853.
- 39 W. A. Staines, D. J. Morassutti, K. R. Reuhl, A. I. Ally and M. W. McBurney, *Neuroscience*, 1994, **58**(4), 735–751.
- 40 A. K. Goetz, B. Scheffler, H. X. Chen, S. S. Wang, O. Suslov, H. Xiang, O. Brustle, S. N. Roper and D. A. Steindler, *Proc. Natl. Acad. Sci. U. S. A.*, 2006, **103**(29), 11063–11068.
- 41 E. Meijering, M. Jacob, J. C. F. Sarria, P. Steiner, H. Hirling and M. Unser, *Cytometry, Part A*, 2004, **58A**(2), 167–176.
- 42 R. Milner and I. L. Campbell, *J. Neurosci. Res.*, 2002, **69**(3), 286–291.
- 43 N. L. Benoiton, *Chemistry of peptide synthesis*, Taylor & Francis, Boca Raton, 2006.
- 44 C. G. Fields, D. H. Lloyd, R. L. Macdonald, K. M. Otteson and R. L. Noble, *Peptide Res.*, 1991, **4**(2), 95–101.